Aalborg Universitet

AALBORG UNIVERSITY
DENMARK

Passivity-based coordinated control for islanded AC microgrid

Gui, Yonghao; Wei, Baoze; Li, Mingshen; Guerrero, Josep M.; Vasquez, Juan C.

AALBORG UNIVERSITY

DENMARK

Passivity-Based Coordinated Control for Islanded AC Microgrid

Gui, Yonghao; Wei, Baoze; Li, Mingshen; Guerrero, Josep M.; Quintero, Juan Carlos Vasquez

Passivity-Based Coordinated Control for Islanded AC Microgrid

Yonghao Gui[1], Baoze Wei, Mingshen Li, Josep M. Guerrero, Juan C. Vasquez

Department of Energy Technology, Aalborg University, 9220 Aalborg, Denmark

Declarations of interest: none

Abstract

A novel passivity-based coordinated control strategy is proposed for an islanded AC microgrid including renewable energy source and energy storage system units. The main advantage is that the proposed coordinated control strategy manages the microgrid without using a phase-locked loop system. In the microgrid, the energy storage system supports the voltage of the microgrid, and the renewable energy sources inject their maximum power to the microgrid in the normal operation. For the energy storage system, we use a proportional-resonant controller, and for the renewable energy sources, we use a voltage modulated direct power control method, which has not only a good tracking performance but also a good steady-state behavior. Another advantage of the proposed method is that the asymptotical stability of the whole microgrid can be guaranteed by using the passivity principle when the heterogeneous renewable energy sources are integrated into the microgrid. To validate the proposed coordinated control law, we use a microgrid consisting of one energy storage system, one wind turbine, one photovoltaic and two controllable loads. Simulation results show that the plug-and-play capability of the wind turbine and photovoltaic in the microgrid is enhanced when comparing with the conventional vector current control method with a phase-locked loop system. Moreover, the voltage and frequency of the microgrid are recovered to its nominal value by the energy storage system with the proposed method as well. Finally, experimental verification of the proposed coordinated control algorithm is performed

---

[1]Email; yog@et.aau.dk.

on a 10 kW microgrid system. The experimental results match the simulation ones as well.

1. Introduction

Nowadays, a revolution of the world energy system is taking place to a low carbon, green, and sustainable one [1]. It introduces new network topologies, the new components, and new design and operation strategies [2]. The wind turbines (WTs), photovoltaic (PV), biomass, tidal power, and hydro are the most important sources in renewable energy resources (RESs) to mitigate greenhouse gas emissions and provide clean energy for sustainable development [3]. Due to the fast development of such RESs, the large-scale RESs have been widely integrated into power distribution systems [4]. However, the volatile and intermittent nature of WT and PV sources may cause serious problems regarding stability and reliability [5]. As the next generation of power grids, the smart power grids require an intelligent strategy to integrate a large number of RESs into a utility grid as a microgrid for reducing system uncertainties and improving performance [6].

Microgrids operate not only in a grid-connected mode to exchange power with the main grid [7], but also in the islanded mode to support local loads when the connection to grid fails [8]. With the rapid development of power converters, the RESs such as PV and WT systems have been the main distributed generation sources in microgrids [9]. Consequently, the microgrid should be able to overcome the volatile and intermittent nature of RESs [10]. Energy storage system (ESS) is considered as an essential and effective solution to enhance the flexibility and controllability not only in specific RESs [11], but also in the microgrid [12]. Hence, the coordinated control is required to guarantee stored energy balance among ESSs and RESs to enhance the stability and reliability of the microgrid system [13].

This coordinated problem has been addressed by centralized control and decentralized control concerning the communication links [14]. In centralized control, as a cru-

cial element, the communication channels can enhance the stability of microgrid [15]. A communication based adaptive droop control for ESSs in a microgrid is proposed to deliver more power regarding its higher state [16]. A coordinated control strategy for state of charge (SoC) balancing in a microgrid has been proposed by combing communication technology with hierarchical control in [17]. However, these control methods will not stabilize the system if communication network occurs failure. Coordinated and integrated control is proposed for PV and battery storage systems regarding V-f (or P-Q) droop control, maximum power point tracking (MPPT) control, and energy storage charging and discharging controls [18]. However, it needs a central control system. In [19], centralized coordinated control is employed for equalizing the SoC, even for distributed ESSs with different capacities. However, the drawback is that the overall system will lose coordination when a single point failure occurs in one of the communication links. Multi-master-slave-based control has been proposed to provide rapid load sharing considering distant groups while using the Conservative Power Theory [20]. *Sun et al.* proposed a power sharing unit based on the adaptive backstepping sliding mode control to achieve the coordinated power sharing in a hybrid microgrid structure [21]. However, there is a tradeoff between synchronization and power-sharing accuracy for the method. Moreover, *Arcos-Aviles et al.* proposed a fuzzy logic-based control strategy to deal with the problem of minimization of fluctuations and power peaks while exchanging energy with the main grid [22]. However, it does not consider the voltage and frequency regulation problem.

It is rapidly changing control and operation of microgrids from a centralized fashion to a decentralized one [23]. In the decentralized control of microgrids, DG units are required to share the total load demand in microgrids based on their power capacities, preferably without communication links [24]. Decentralized coordinated control for balancing discharge rate of ESSs in an islanded microgrid is an effective method to prevent overcurrent and unintentional outage of RES units, and to provide fast response and large stability margin [25]. Another decentralized control method is proposed by detection of load change time in the microgrid [26]. In [27], autonomous real power control strategy is proposed to realize decentralized power management, which relies on local controllers without external communication links. Independent control is im-

3

plemented in each unit using multi-loop controllers to autonomously supply power only during peak load periods and keep power balance [28]. However, the control conditions are based on the PV system, while the multiple RESs are still not considered. In [29], coordinated control strategy is investigated to control the power of islanded units flexibly by applying smooth switching droop control. However, it needs a complex computation and additional microgrid management for ensuring reliable operation. Recently, some distributed control methods are also proposed to enhance the performance of the microgrids. A distributed generation control method is proposed for accurate real power sharing and self-frequency recovery [30]. *Xu* and *Sun* propose an adaptive virtual impedance control to obtain an improved real/reactive power sharing [31]. Moreover, distributed cooperative control using feedback linearization [32], distributed-averaging proportional–integral controller [33], dynamic consensus algorithm [34], droop-free distributed method [35], fuzzy Q-learning for multi-agent method [36], and consensus-based distributed coordination approach [37] are proposed to achieve bounded voltage and accurate reactive power sharing in microgrids.

The aforementioned methods use a phase-locked loop (PLL) for synchronization when RESs are integrated into the existing microgrids. Moreover, stability analysis of the microgrids will become complex when the heterogeneous RESs are integrated. To deal with these problems, in this paper, a novel coordinated control strategy applied to RES/ESS units is proposed in islanded microgrids without using PLL. The ESS is operating to support the voltage and frequency in the microgrid, and the RESs are operating to inject their maximum power to the microgrid. For the ESS, it uses a conventional proportional-resonant (PR) controller [38], and for the RES, we use a voltage modulated direct power control (VM-DPC), which has not only a good tracking but also steady-state performances [39]. One of the objective of the paper is that to remove the synchronization process to improve the plug-and-play capability of RESs. The VM-DPC enhances the plug-and-play capability of RESs since they are integrated into the existing microgrids without using the PLL. It means that there is no synchronization process, and we can expect the improved performance of the plug-and-play capability of RESs.

Another objective is that the stability of the microgrids is to be guaranteed when

the heterogeneous RESs are integrated into the microgrid. To ensure the stability of the microgrid, we use the passivity property, which has an advantage that if a group of passive sub-systems is connected through paralleling or feedback, the whole system is also stable and passive [40]. That is if each RES plugs-in to the whole microgrid and satisfies passivity, the asymptotical stability of the microgrid can be guaranteed by using the passivation [41]. Hence, we use the port-controlled Hamiltonian (PCH) for RESs to get the passivity properties when the VM-DPC is used. To validate the proposed coordinated control law, we use a microgrid consisting of one ESS, one WT, one PV and controllable loads. Simulation and experiment results show that the islanded microgrid is operating well and the plug-and-play capability of the WT and PV is enhanced. Compare to the conventional vector current control method with a PLL system, the proposed control strategy shows an improved performance when the RESs are connected to the microgrid in the simulation results. Moreover, the voltage and frequency of the microgrid could be recovered to its nominal value by the ESS with the proposed control strategy as well. In the future, we will design a secondary controller for this coordinated control architecture with consideration of SoC for the ESS.

The rest of the paper is organized as follows. In Section 2, the conventional PR controller and the VM-DPC are briefly introduced. Section 3 presents the stability analysis for microgrids including RESs. Section 4 shows the case studies through MATLAB/Simulink, Simscape Power Systems, and we also validate the proposed method by using a 10 kW microgrid system in Section 5. Finally, the conclusions are given in Section 6.

2. Review of PR and VM-DPC

In this Section, we briefly introduce PR and VM-DPC controllers. The PR controller is used for the ESS to fix the voltage and frequency in the microgrid, and the VM-DPC is used for RESs, which will inject its maximum power to the microgrid.

2.1. PR controller

For controlling an AC signal, the PR controller is an effective method to track the reference without steady-state error comparing with PI control. The transfer function
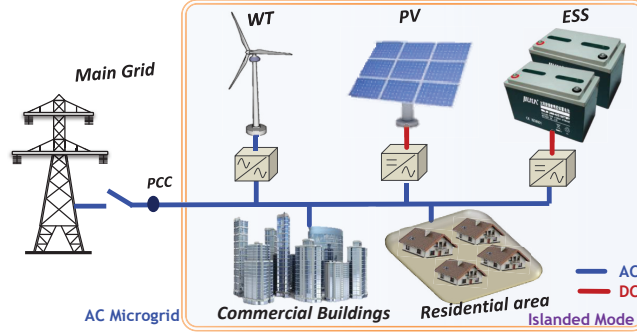
5

Figure 1: Architecture of an islanded AC microgrid

of the ideal PR controller can be expressed as follows:

$$G(s) = K_P + \frac{K_R s}{s^2 + \omega_0^2}, \tag{1}$$

where ω_0 is the angular frequency. K_P and K_R are the controller gains. The controller has an infinite gain at the frequency ω_0, and there is no phase shift and gain at other frequency. K_P is able to determine the dynamics of the system regarding bandwidth, phase and gain margin [38]. Besides fundamental frequency compensation, the harmonic compensation can be obtained by cascading several generalized integrators tuned to resonate at the desired frequency. For example, the transfer control of harmonic compensator designed to compensate the 3rd, 5th and 7th harmonics is given as follows:

$$G_h(s) = \sum_{h=3,5,7} \frac{K_{ih} s}{s^2 + (\omega_0 \times h)^2}, \tag{2}$$

where K_{ih} is the controller gain. Thus, the harmonic compensator works on both positive and negative sequences of the selected harmonic, which only reacts to the frequency very close to the resonant frequency. The enhanced tracking performances are employed widely for grid-connected inverter control. For the simplification, we use the PR controller for the ESS to support the voltage for the microgrid as shown in Fig. 2. The references of the voltage and frequency of the microgrid are given to the PR controller of the ESS.
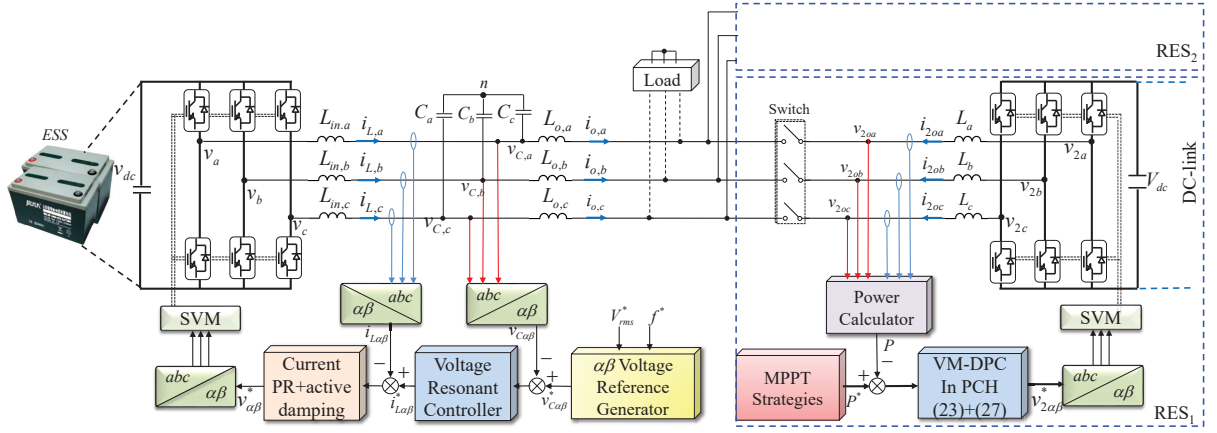
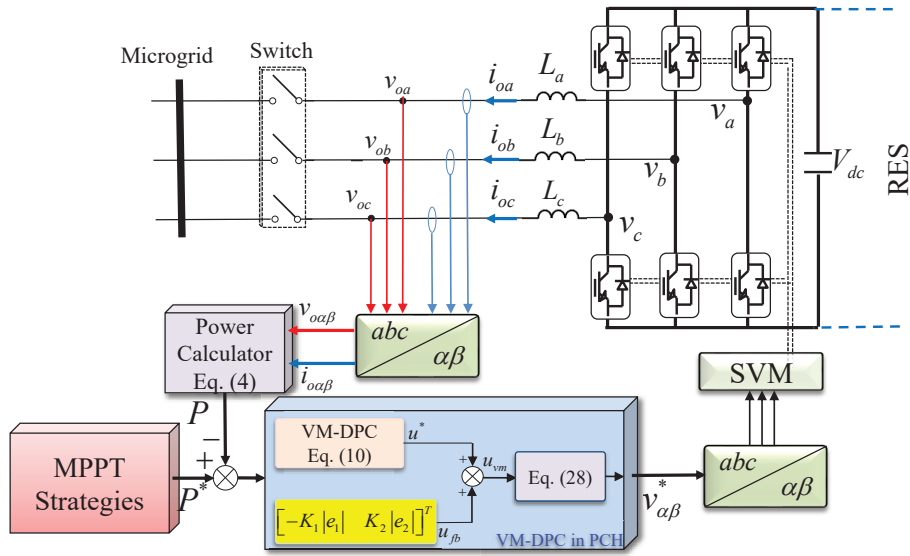Figure 2: Control block diagram of the passivity-based coordinated control for RESs and ESS.

Figure 3: Controller block diagram of RES.

2.2. VM-DPC of RES

Fig. 2 shows that two RESs are connected to the microgrid through an inverter with an L-filter. Considering a balanced grid voltage condition, the dynamics of line current in α-β reference frame are represented as follows [42]:

$$
\begin{aligned}
v_\alpha &= Ri_{o\alpha} + L\frac{di_{o\alpha}}{dt} + v_{o\alpha}, \\
v_\beta &= Ri_{o\beta} + L\frac{di_{o\beta}}{dt} + v_{o\beta},
\end{aligned}
\tag{3}
$$

where $i_{o\alpha}$, $i_{o\beta}$, v_α, v_β, $v_{o\alpha}$, and $v_{o\beta}$ represent the line currents, converter voltages, and grid voltages in $\alpha - \beta$ frame, respectively. L and R are the filter inductance and resistance, respectively. We define the instantaneous real and reactive powers as follows [43]:

$$
\begin{aligned}
P &= \frac{3}{2}(v_{o\alpha}i_{o\alpha} + v_{o\beta}i_{o\beta}), \\
Q &= \frac{3}{2}(v_{o\beta}i_{o\alpha} - v_{o\alpha}i_{o\beta}),
\end{aligned}
\tag{4}
$$

where P and Q are the instantaneous output real and reactive powers, respectively. With consideration of a nondistorted grid, the dynamics of the instantaneous real and reactive powers could be obtained based on the grid voltage variations as follows:

$$
\begin{aligned}
\frac{dP}{dt} &= -\frac{R}{L}P - \omega Q + \frac{3}{2L}(v_{o\alpha}v_\alpha + v_{o\beta}v_\beta - V_g^2), \\
\frac{dQ}{dt} &= \omega P - \frac{R}{L}Q + \frac{3}{2L}(v_{o\beta}v_\alpha - v_{o\alpha}v_\beta),
\end{aligned}
\tag{5}
$$

where ω is the angular velocity of the voltage and $V_g = \sqrt{v_{o\alpha}^2 + v_{o\beta}^2}$. Define two states and two control inputs as $x = \begin{bmatrix} x_1, x_2 \end{bmatrix}^T = \begin{bmatrix} P, Q \end{bmatrix}^T \in X_o \subset \mathbb{R}^2$, $u = \begin{bmatrix} u_1, u_2 \end{bmatrix}^T = \begin{bmatrix} v_\alpha, v_\beta \end{bmatrix}^T \in U_o \subset \mathbb{R}^2$, where X_o and U_o are the compact sets in the operating range. Then, a continuous dynamic model of an RES in state-space is represented as follows:

$$
\begin{aligned}
\dot{x} &= \begin{bmatrix} -\frac{R}{L}x_1 - \omega x_2 + \frac{3}{2L}(v_{o\alpha}u_1 + v_{o\beta}u_2 - V_g^2) \\ \omega x_1 - \frac{R}{L}x_2 + \frac{3}{2L}(v_{o\beta}u_1 - v_{o\alpha}u_2) \end{bmatrix}, \\
y &= \begin{bmatrix} x_1 & x_2 \end{bmatrix}^T.
\end{aligned}
\tag{6}
$$

We define a VM control inputs [44]:

$$
u_{vm} = \begin{bmatrix} u_{vm1} \\ u_{vm2} \end{bmatrix} = \begin{bmatrix} v_{o\alpha}u_1 + v_{o\beta}u_2 \\ -v_{o\beta}u_1 + v_{o\alpha}u_2 \end{bmatrix}.
\tag{7}
$$

8

Consequently, the original system (6) can be rewritten as follows:

$$\dot{x} = \begin{bmatrix} -\frac{R}{L}x_1 - \omega x_2 + \frac{3}{2L}(u_{vm1} - V_g^2) \\ \omega x_1 - \frac{R}{L}x_2 - \frac{3}{2L}u_{vm2} \end{bmatrix}.$$ (8)

For tracking performance, we define an error vector such as

$$e := x^* - x = \begin{bmatrix} e_1 \\ e_2 \end{bmatrix} = \begin{bmatrix} x_1^* - x_1 \\ x_2^* - x_2 \end{bmatrix},$$ (9)

where $x^* = \begin{bmatrix} x_1^* & x_2^* \end{bmatrix}^T$ denotes the reference.

Theorem 1. *[45] Consider the system* (8), *if we take a control law such as*

$$u_{vm} = \begin{bmatrix} u_{vm1} \\ u_{vm2} \end{bmatrix} = \begin{bmatrix} V_g^2 + \frac{2R}{3}x_1 + \frac{2L\omega}{3}x_2 + v_1 \\ \frac{2L\omega}{3}x_1 - \frac{2R}{3}x_2 - v_2 \end{bmatrix},$$ (10)

and v_1 and v_2 can be designed as follows:

$$v_1 = K_{P,p}e_1 + K_{P,i}\int_0^t e_1(\tau)d\tau,$$

$$v_2 = K_{Q,p}e_2, + K_{Q,i}\int_0^t e_2(\tau)d\tau,$$ (11)

where $K_{P,p}$, $K_{Q,p}$, $K_{P,i}$, and $K_{Q,i}$ are the positive gains, then the errors globally exponentially converge to zeros. ◊

Proof: We differentiate each output until at least one of the control inputs appears.

$$\begin{bmatrix} \dot{y}_1 \\ \dot{y}_2 \end{bmatrix} = \begin{bmatrix} -\frac{R}{L}x_1 - \omega x_2 + \frac{3}{2L}(u_{vm1} - V_g^2) \\ \omega x_1 - \frac{R}{L}x_2 - \frac{3}{2L}u_{vm2} \end{bmatrix}.$$ (12)

If, the control inputs u_{vm1} and u_{vm2} are taken as (10), then the output is

$$\dot{y}_1 = v_P, \quad \dot{y}_2 = v_Q.$$ (13)

To simplify the analysis, we assume that $\dot{x}_1^* = 0$ and $\dot{x}_2^* = 0$. Consequently, taking the new control law as (11) gives us two simple decoupled error dynamics for real and reactive powers.

$$\dot{e}_1 = -K_{P,p}e_1 - K_{P,i}\int_0^t e_1(\tau)d\tau,$$

$$\dot{e}_2 = -K_{Q,p}e_2 - K_{Q,i}\int_0^t e_2(\tau)d\tau.$$ (14)

It is obvious that the closed-loop system is globally exponentially stable. □

3. Stability Analysis

In this Section, we discuss the stability of the microgrid. The various methods of the stability analysis for the microgrids have been researched [46]. In [47], a small-signal model of a microgrid is studied. The stability of the DC microgrid is guaranteed by using the passivation in [41]. In this paper, we guarantee the stability of the whole AC microgrid via the passivity property, which has an advantage that the whole system is stable and passive if a group of passive sub-systems is connected through paralleling or feedback. At first, we briefly introduce a port-controlled Hamiltonian (PCH) system, which satisfies passivity property [48]. Then, we use the PCH for RESs to get the passivity property when the VM-DPC is applied to the RES.

3.1. Port-Controlled Hamiltonian (PCH) System

Let $x \in \mathbb{R}^n$ denotes the state vector and $u \in \mathbb{R}^m$ denotes the input. Consider a system described in the state space as

$$\dot{x} = f(x, u), \tag{15}$$

where $x \in X \subset \mathbb{R}^n$ is the state vector, and $u \in U \subset \mathbb{R}^m$ is the input. The function $f(\cdot, \cdot) : X \times U \to \mathbb{R}^n$ is sufficiently smooth in the open connected set X. Suppose that (15) satisfies a PCH system as follows:

$$\dot{x} = (\mathfrak{J} - \mathfrak{R}) \frac{\partial H(x)}{\partial x} + G(u), \tag{16}$$

where H is the Hamiltonian function given by

$$H(x) = \frac{1}{2} x^T S x, \quad S = S^T \succ 0,$$
$$\mathfrak{J}^T = -\mathfrak{J}, \quad \mathfrak{R} = \mathfrak{R}^T \succ 0. \tag{17}$$

Here, $\succ$ indicates positive definite, the matrices S and $\mathfrak{R}$ are constant $n \times n$ matrices. $\mathfrak{R}$ indicates the dissipative forces in the system, $\mathfrak{J}$ represents the conservative forces, and $G(u)$ represents the energy acquisition term [49, 50].

Assumption 1. Suppose that there exist signals $u^d(t)$ and $x^d(t)$ that satisfy the PCH form (16):

$$\dot{x}^d = (\mathfrak{J} - \mathfrak{R}) \frac{\partial H(x^d)}{\partial x^d} + G(u^d). \tag{18}$$

$\diamondsuit$

In this paper, we consider that the system dynamics are sufficiently smooth in the open connected set X., thus Assumption 1 is acceptable in this study.

Theorem 2. *Suppose a system has the PCH form in* (16) *and has a reference trajectory $x^d(t)$ that satisfies* (18). *If $u = u^d$ is applied to the system in* (16), *then the closed-loop system is exponentially stable. Namely,* $\lim_{t \to \infty} x(t) = x^d(t)$. $\diamondsuit$

Proof: Let $x(t) \in X \subset \mathbb{R}^n$ be the trajectory of (16) corresponding to $u = u^d \in U \subset \mathbb{R}$ such that

$$\dot{x} = \left(\mathfrak{J}(u^d) - \mathfrak{R} \right) \frac{\partial H(x)}{\partial x} + G(u^d).$$

Although $x(t)$ and $x^d(t)$ satisfy the same dynamics equations, but they are not the same signals because their initial conditions could be different. By defining the error as $e := x^d - x$, we obtain the following tracking error dynamics:

$$\dot{e} = \dot{x}^d - \dot{x} = \left(\mathfrak{J}(u^d) - \mathfrak{R} \right) \frac{\partial H(e)}{\partial e}.$$

Let us use $H(e)$ as a Lyapunov function candidate, where H is defined in (17). The total time derivative of $H(e)$ is given by

$$\dot{H}(e) = \frac{1}{2} \left(\dot{e}^T \left(\frac{\partial H(e)}{\partial e} \right) + \left(\frac{\partial H(e)}{\partial e} \right)^T \dot{e} \right)$$
$$= -e^T S^T \mathfrak{R} S e.$$

Since $S = S^T \succ 0$ and $\mathfrak{R} \succ 0$, the equilibrium point at the origin of the error dynamics is globally exponentially stable. Hence, $\lim_{t \to \infty} \| x^d(t) - x(t) \| = 0$. $\square$

Remark 1. *x and x^d have the same dynamics but may have different initial conditions.*

u^d could be obtained if we use the flatness property. However, to use the advantages of the VM-DPC, the following analysis is addressed.

3.2. VM-DPC with PCH

In this study, the dynamics in (8) also satisfy the PCH form in (16). For the system (8), if we take a Hamiltonian function such that

$$H(x) = \frac{1}{2} x^T S x \tag{19}$$

11

where $S = I_2$, then the system in (8) is changed into the PCH form in (16) as follows:

$$\dot{x} = (\mathfrak{J} - \mathfrak{R}) \frac{\partial H(x)}{\partial x} + G(u), \tag{20}$$

where

$$\mathfrak{J} = \begin{bmatrix} 0 & \omega \\ -\omega & 0 \end{bmatrix}, \mathfrak{R} = \begin{bmatrix} \frac{R}{L} & 0 \\ 0 & \frac{R}{L} \end{bmatrix}, G(u) = \begin{bmatrix} \frac{3}{2L}(u_{vm1} - V_g^2) \\ \frac{3}{2L}u_{vm2} \end{bmatrix}.$$

Assumption 2. We define VM-DPC in (10) as u^*, suppose that using u^*, x converges to x^* that has a relationship with x^d of (18) as follows:

$$x^d - x^* = \begin{bmatrix} \exp^{-\lambda_1 t}(x_1^d - x_1) \\ \exp^{-\lambda_2 t}(x_2^d - x_2) \end{bmatrix}. \tag{21}$$

where $\lambda_{1,2}$ are the decay ratio of each state. $\Diamond$

Assumption 2 is acceptable in this study, since from Theorem 1, we conclude that the closed loop system is globally exponentially stable. Regarding Assumptions 1 and 2, we can get the relationship between the desired controller in (18), u^d, and VM-DPC in (10), $u^* = u_{vm}$, as follows:

$$\begin{aligned} \delta u_1 = u_1^d - u_1^* = \frac{3\exp^{-\lambda_1 t}}{2L}\left(-\lambda_1 \dot{e}_1 + \frac{R}{L}e_1 + \omega e_2\right), \\ \delta u_2 = u_2^d - u_2^* = \frac{3\exp^{-\lambda_2 t}}{2L}\left(\lambda_2 \dot{e}_2 - \frac{R}{L}e_2 + \omega e_1\right), \end{aligned} \tag{22}$$

where λ_1 and λ_2 are the decay ratio of e_1 and e_2, respectively. .

Assumption 3. Suppose that $\forall x \in X_o$, where X_o is operating range, there exist Δ_1 and Δ_2 that satisfy:

$$\sup_{\forall x \in X_o} \dot{e}_1 = \Delta_1, \quad \sup_{\forall x \in X_o} \dot{e}_2 = \Delta_2. \tag{23}$$

$\Diamond$

Due to the rated power of converters and RESs, the powers generated from the RESs to the microgrid are bounded. Moreover, the states are stabilized and regulated in the operating range via the VM-DPC. Consequently, e and $\dot{e}$ are also be bounded with the given reference. Consequently, Assumption 3 is acceptable in this study.

Theorem 3. *Given dynamic system* (8), *suppose that the Assumptions 1 to 3 hold. If the control input is designed with VM-DPC* (10) *and a new feedback such as*

$$\hat{u}_{vm} = u^* + u_{fb}, \tag{24}$$

where $u_{fb} = \left[-\kappa_1|e_1|, \kappa_2|e_2| \right]^T$ *with* $\kappa_1 \geq \lambda_1\Delta_1$ *and* $\kappa_2 \geq \lambda_2\Delta_2$, *then the tracking error of* (8) *based on the PCH form is exponentially stabilized.*   ◇

Proof: Let us consider a Lyapunov function candidate such as

$$V(e) = \frac{1}{2}e^T Se > 0. \tag{25}$$

The derivative of (25) with respect to time results in

$$\dot{V}(e) = \frac{1}{2}\left(\dot{e}^T\left(\frac{\partial H(e)}{\partial e} \right) + \left(\frac{\partial H(e)}{\partial e} \right)^T \dot{e} \right) \tag{26}$$

$$= -e^T \Re e + \delta u_1 e_1 + \delta u_2 e_2 - \kappa_1|e_1| - \kappa_2|e_2|.$$

Using (22), (26) can be rewritten as follows:

$$\dot{V}(e) \leq -\lambda_1 \exp^{-\lambda_1 t} \dot{e}_1 e_1 - \lambda_2 \exp^{-\lambda_2 t} \dot{e}_2 e_2 - \kappa_1|e_1| - \kappa_2|e_2| \tag{27}$$

$$\leq -\varepsilon_1|e_1| - \varepsilon_2|e_2| < 0,$$

where $\varepsilon_1 \geq \kappa_1 - \lambda_1\Delta_1$ and $\varepsilon_2 \geq \kappa_2 - \lambda_2\Delta_2$. Thus the tracking error of (8) in the PCH form is exponentially stabilized.   □

Finally, based on (7) and (24), the original control inputs are calculated.

$$v_\alpha = \frac{v_{o\alpha}u_{vm1} - v_{o\beta}u_{vm2}}{V_g^2},$$

$$v_\beta = \frac{v_{o\beta}u_{vm1} + v_{o\alpha}u_{vm2}}{V_g^2}. \tag{28}$$

Remark 2. *To guarantee the passivity property of the ESS, we modified the PR controller with active damping, which was designed in [51].*

Fig. 3 shows the block diagram of the proposed method. In normal operation, RES will generate its maximum power. Hence, we assume that RESs are operated in MPPT

Table 1: System parameters used in simulation

Parameter	Symbol	Value	Unit
Nominal bus voltage	V^*_{rms}	230	V
Nominal bus frequency	f^*	50	Hz
Filter inductance of ESS	L_{in}	1.8	mH
Filter capacitor of ESS	C	9×3	μF
Output inductance of ESS	L_o	1.8	mH
Filter inductance of PV & WT	L_{pv}&L_{wt}	3.6	mH

mode in this study. Based on Theorem 3, the integrated RESs have the passivity property. Consequently, the stability of the whole microgrid can be guaranteed by using the passivity principle [40], *i.e.* the whole system including the ESS and RESs is asymptotically stable.

4. Simulation Results

To validate the proposed coordinated control method, we use MATLAB/Simulink, Simscape Power Systems. The microgrid selected as a case study is modified from the one discussed in [52], where a lab-scale prototype is used based a real microgrid platform implemented in Shanghai [53]. The parameters of the tested system are listed in Table 1. The ESS supports the bus voltage and frequency for the microgrid and the WT and PV inject their MPPT powers to the microgrid, as shown in Fig. 4. The VSCs of the ESS and the RESs are used through the switched model in Simscape Power Systems library, and the proposed control strategy is implemented by using Simulink library.

Fig. 5 describes the power tracking performance when the WT, PV, loads 1&2 are connected to the microgrid. At first, the ESS generates and maintains the bus voltage and frequency of the microgrid. At 0.2 s, the switch S_1 is on, and the load 1 is connected to the microgrid. At this time, only ESS injects the real power to the microgrid to balance the generation and consumption. Suddenly, the switch S_2 turns on at 0.51 s, and the WT is connected to the microgrid and generates 6 kW. For this connection,
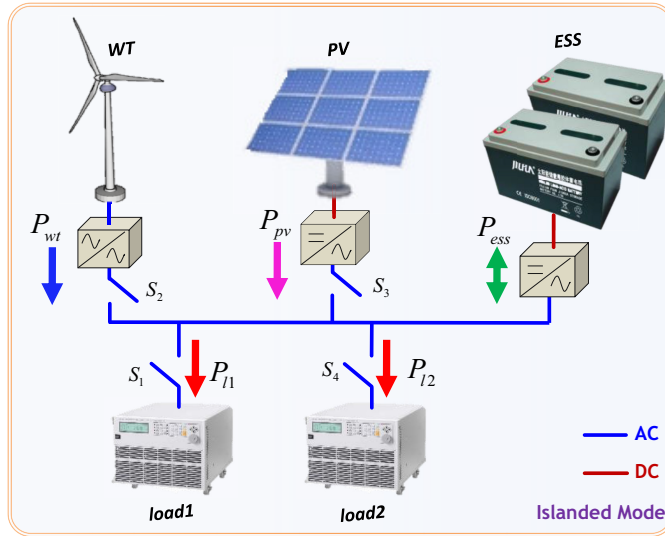
Figure 4: Electrical scheme used in the simulation.

the WT does not require a synchronization process. Fig. 7(c) and (d) show the currents of the ESS and WT at 0.51 s, and the WT is connected and injects the currents to the microgrid simultaneously. The WT supports all the power consumed at the load and the surplus power is flowing into the ESS for its charging, as shown in Fig. 5 (a). The voltages and currents of the load 1 have a small overshoot and converge to their operating points in one cycle, as shown in Fig. 8(c) and (d). To compare the performance, we use a conventional method, which uses a vector current control designed in the d–q frame with a PLL system. Fig. 7(b) shows that the currents of WT with the conventional method have a larger overshoot than those with the proposed method when the WT is connected and injects the currents to the microgrid simultaneously, since there is a synchronization process with the conventional method. The PLL system estimates the phase angle of the grid voltage slowly due to the slow dynamics of the PLL system. We can increase the bandwidth of the PLL system to improve the dynamic performance. However, increasing the bandwidth of the PLL system will cause a unstable phenomenon in a weak grid as discussed in [54]. Hence, we could not increase the bandwidth too much. Such overshoot affects the currents and voltages of the load as well, as shown in Fig. 8(a) and (b). Moreover, the protection system of the inverter may
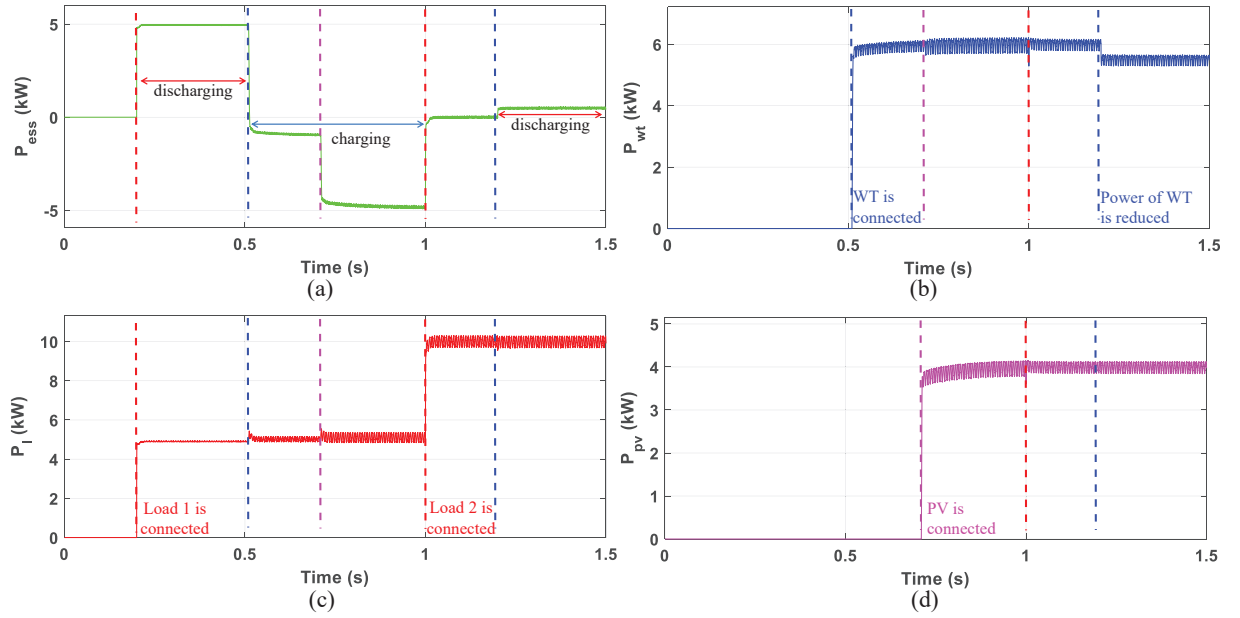
15

Figure 5: The performance of real power of the proposed coordinated control for the islanded AC microgrid: (a) ESS, (b) WT, (c) load, (d) PV.

be activated due to the larger overshoot of the currents when doing some experimental test.

After 0.2 s, the PV is suddenly connected to the microgrid and generates 4 kW. For this connection, the power ripples in the microgrid are slightly increased, and the real power of the load 1 has a slight overshoot, since the voltages and currents of the load are affected by the connection of the PV as shown in Fig. 6. At this time, the PV also does not require the synchronization process. The ESS absorbs the extra powers to maintain the voltage and frequency in the microgrid. Moreover, at 1 s, another load (5 kW) is connected to the microgrid, and the total power of the RESs is equal to the total power of the loads. Consequently, the ESS only supports the voltage and frequency in the microgrid with 0 power regulation, as shown in Fig. 5 (a). Fig. 9 shows that the voltages and currents converge to their operating points fast, but the connection of the load 2 affects the WT and PV which have a slight undershoot, as shown in Figs. 5 (b)
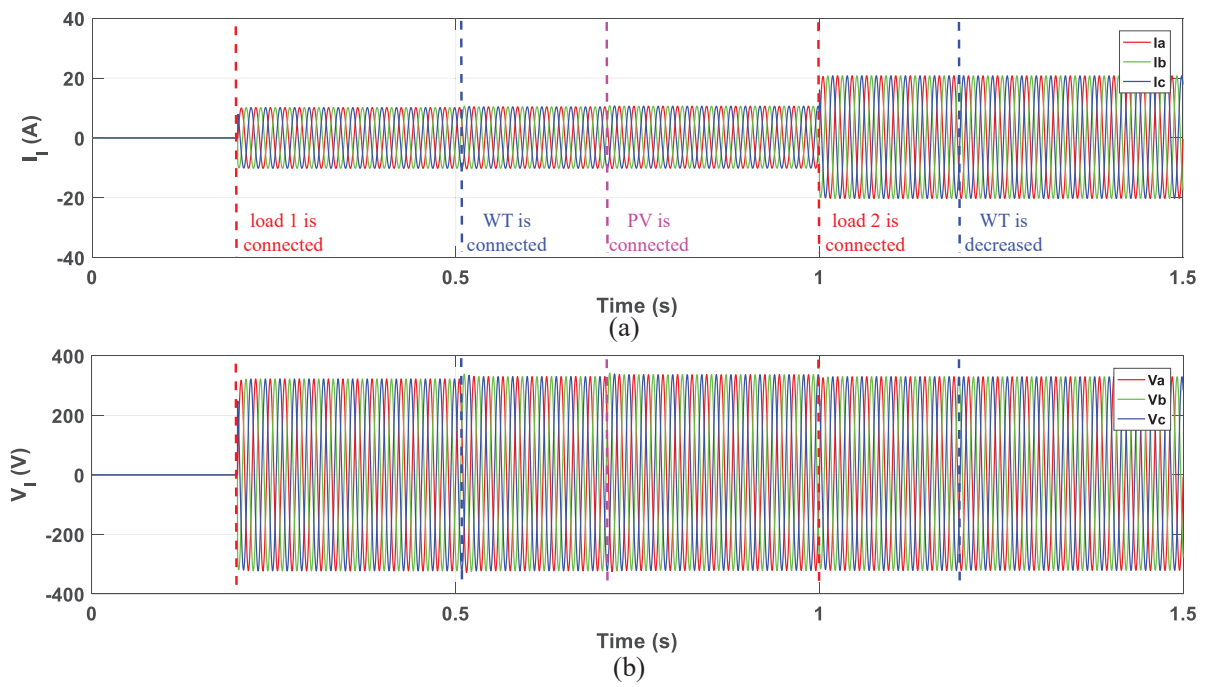
16

Figure 6: Injected currents and voltages of the whole loads. (a) Currents, (b) voltages.
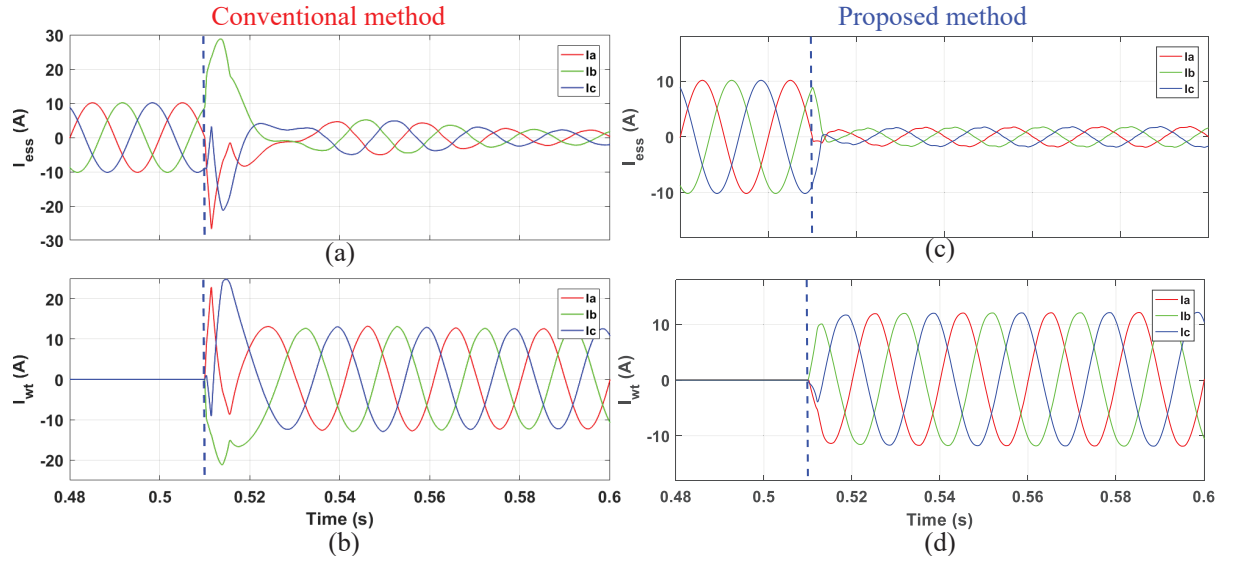
Figure 7: Conventional method: currents of (a) ESS, (b) WT; Proposed method: currents of (c) ESS, (d) WT when the WT is connected at 0.51s.

and (d). Finally, the power of WT is decreased because of the wind at 1.2s, as shown in Fig. 10. Thus, the ESS injects more power into the grid to maintain the voltage and frequency.

Fig. 11 shows the frequency of the microgrid when the WT, PV and the load 2 are connected and the power of WT is reduced. The frequency of the microgrid is recovered to its nominal value by the ESS. Moreover, the THD of voltages and currents of the load are less than 5% as commonly required for grid operation [55]. Consequently, we can conclude that the proposed coordinated control for the islanded microgrid has a good effect and the RES could plug into the microgrid anytime.

5. Experimental Results

We also validate the proposed method with the experimental setup, as shown in Fig. 12. The experimental system parameters are the same as in Table 1, but the voltage of ESS is set to 110 V. Note that one of the inverter emulates an ESS system,
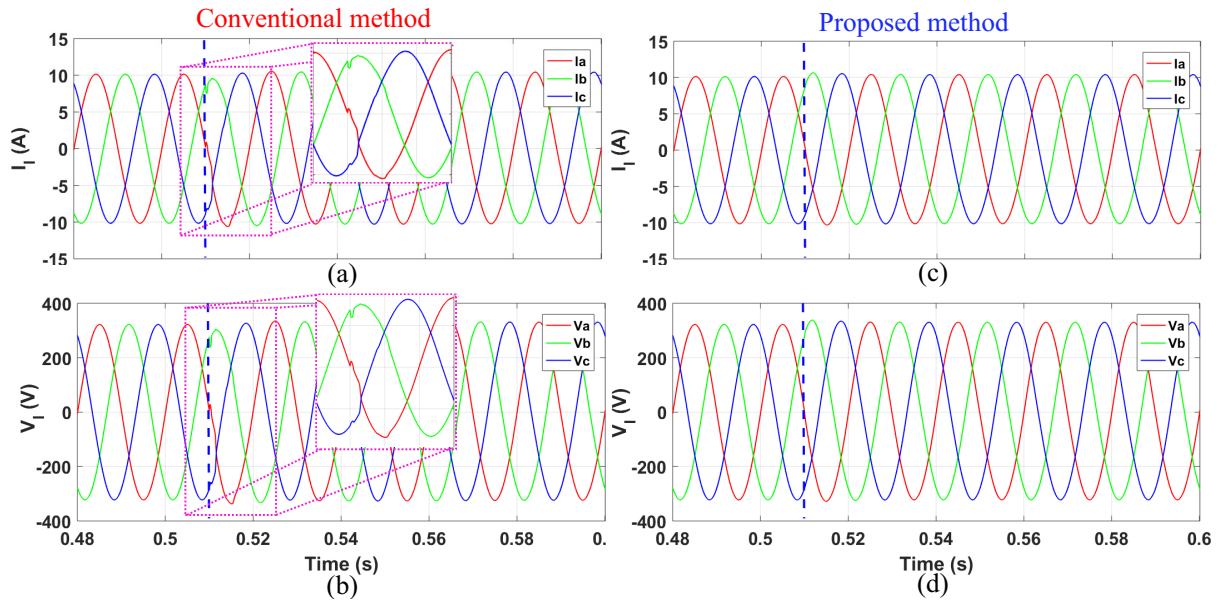
18

Figure 8: Performance of the load 1 when the WT is connected at 0.51s. Conventional method: (a) currents, (b) voltages; Proposed method: (c) currents, (d) voltages.
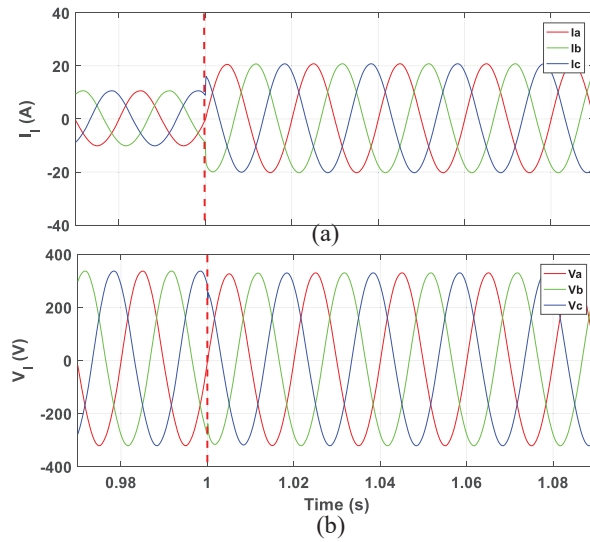

Figure 9: Performance of the whole loads when the load 2 is connected to the microgrid. (a) Currents, (b) voltages.
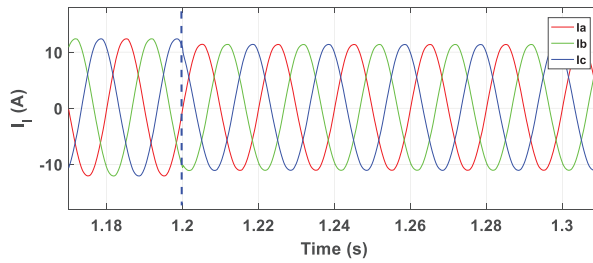
19

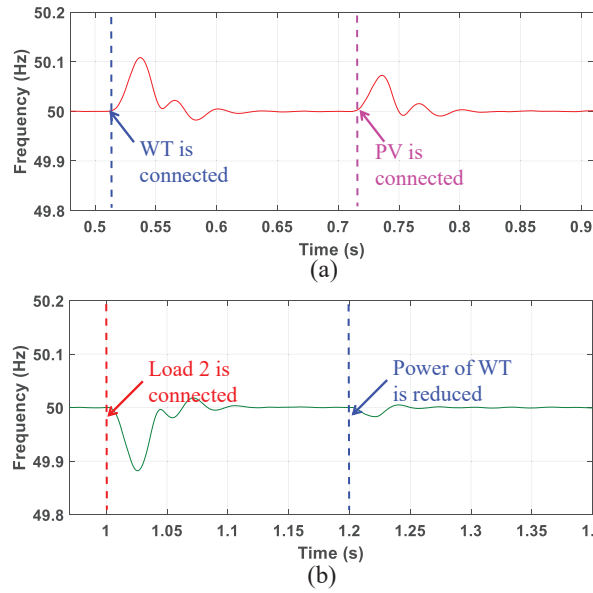Figure 10: Currents of the WT when the power of WT is reduced at 1.2 s.

(a)

(b)

Figure 11: Frequency of the microgrid (a) when the WT and PV are connected; (b) when the load 2 is connected and the WT is reduced.
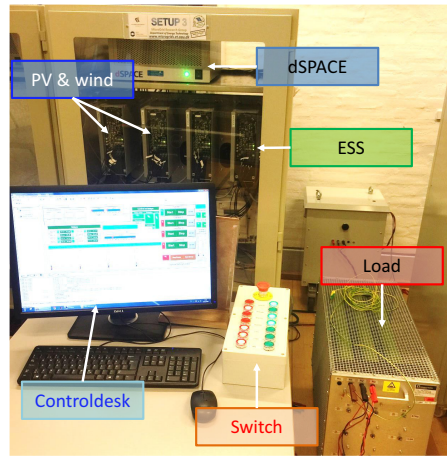
Figure 12: Experimental setup in the laboratory.

and the other two inverters emulate WT and PV, respectively. All the controllers are implemented in the dSPACE 1006 system.

Fig. 13 shows the real power of the ESS and RESs. At first, the ESS supports voltage and frequency to a three-phase load. At 1.85 s, the WT is connected and injects 0.7 kW power to the microgrid, as shown in Fig. 13. The ESS reduces its power to keep the voltage of the load, as shown in Fig. 13 (a). At 2.85 s, the PV is connected and injects 0.4 kW power to the microgrid, as shown in Fig. 13 (d), while the ESS absorbs the power to keep the voltage of the loads, as shown in Fig. 13 (a) and Fig. 14 (c).

6. Conclusions

A novel coordinated control applied to renewable energy source and energy storage system units was proposed to deal with the synchronization problem without phase-locked loop system and stability issues in islanded microgrids . The energy storage system using the conventional proportional resonant controller supports the voltage and frequency of the microgrid, and the renewable energy sources are injecting their maximum power to the microgrid in the normal operation by using the voltage modulated direct power control, which enhances their plug-and-play capabilities since they are integrated into the existing microgrids without using the phase-locked loop system.
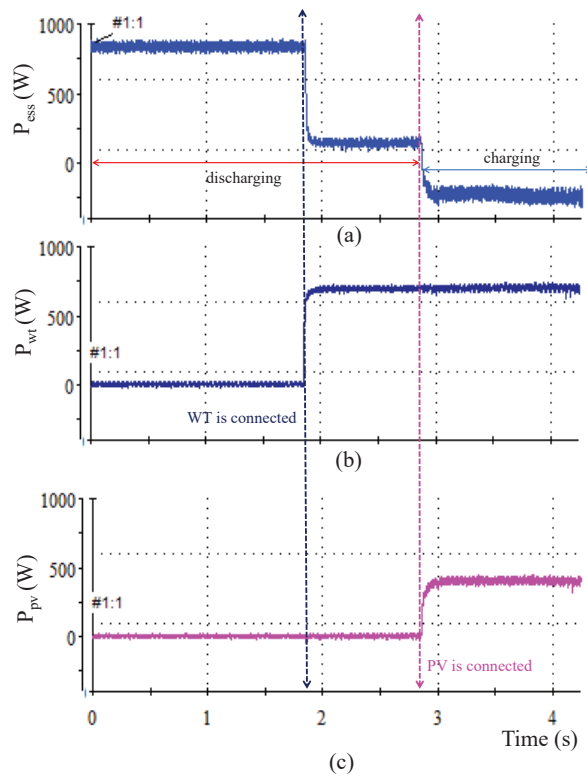
Figure 13: The experimental results of real power of the proposed coordinated control for the islanded microgrid: (a) ESS, (b) WT, and (c) PV.
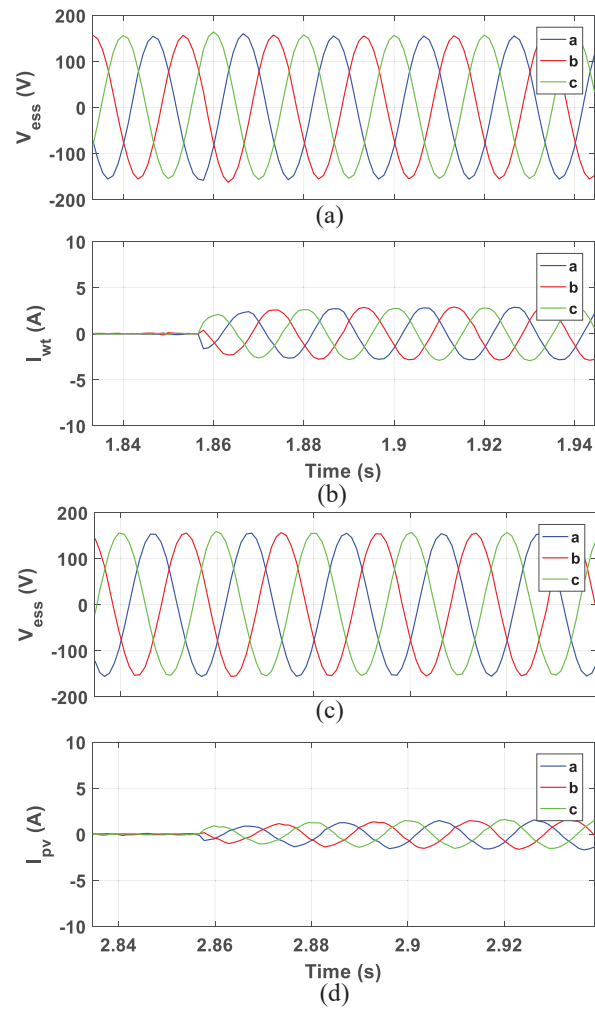
Figure 14: (a) Voltage of ESS and (b) current of WT when the WT is connected; (c) voltage of ESS and (d) current of PV when the PV is connected.

Moreover, we used the passivity property to guarantee the stability of the microgrid. Simulation and experimental results show that the islanded microgrid is operating well and the plug-and-play capabilities of the renewable energy sources are enhanced when comparing with the conventional method.

Acknowledgment

References

[1] E. Mengelkamp, J. Gärttner, K. Rock, S. Kessler, L. Orsini, C. Weinhardt, Designing microgrid energy markets: A case study: The Brooklyn Microgrid, Applied Energy 210 (2018) 870–880.

[2] J. Wu, J. Yan, H. Jia, N. Hatziargyriou, N. Djilali, H. Sun, et al., Integrated energy systems, Applied Energy 167 (2016) 155–157.

[3] H. Hu, N. Xie, D. Fang, X. Zhang, The role of renewable energy consumption and commercial services trade in carbon dioxide reduction: Evidence from 25 developing countries, Applied Energy 211 (2018) 1229–1244.

[4] M. F. Zia, E. Elbouchikhi, M. Benbouzid, Microgrids energy management systems: A critical review on methods, solutions, and prospects, Applied Energy 222 (2018) 1033 – 1055.

[5] D. I. Makrygiorgou, A. T. Alexandridis, Distributed stabilizing modular control for stand-alone microgrids, Applied Energy 210 (2018) 925–935.

[6] C. Wang, J. Yan, C. Marnay, N. Djilali, E. Dahlquist, J. Wu, H. Jia, Distributed energy and microgrids (DEM), Applied Energy 210 (2018) 685 – 689.

[7] J. M. Guerrero, J. C. Vasquez, J. Matas, L. G. De Vicuña, M. Castilla, Hierarchical control of droop-controlled AC and DC microgrids—A general approach toward standardization, IEEE Trans. Ind. Electron. 58 (1) (2011) 158–172.

[8] S. Riverso, M. Tucci, J. C. Vasquez, J. M. Guerrero, G. Ferrari-Trecate, Stabilizing plug-and-play regulators and secondary coordinated control for AC islanded microgrids with bus-connected topology, Applied Energy 210 (2018) 914–924.

[9] L. H. Koh, P. Wang, F. H. Choo, K.-J. Tseng, Z. Gao, H. B. Püttgen, Operational adequacy studies of a PV-based and energy storage stand-alone microgrid, IEEE Trans. Power Syst. 30 (2) (2015) 892–900.

[10] M. Nehrir, C. Wang, K. Strunz, H. Aki, R. Ramakumar, J. Bing, Z. Miao, Z. Salameh, A review of hybrid renewable/alternative energy systems for electric power generation: Configurations, control, and applications, IEEE Trans. Sustain. Energy 2 (4) (2011) 392–403.

[11] H. Zhao, Q. Wu, S. Hu, H. Xu, C. N. Rasmussen, Review of energy storage system for wind power integration support, Applied Energy 137 (2015) 545–553.

[12] J. Wu, C. Zhang, Z. Chen, An online method for lithium-ion battery remaining useful life estimation using importance sampling and neural networks, Applied energy 173 (2016) 134–140.

[13] J. Hu, Y. Xu, K. W. Cheng, J. M. Guerrero, A model predictive control strategy of PV-Battery microgrid under variable power generations and load conditions, Applied Energy 221 (2018) 195–203.

[14] M. Ashabani, H. B. Gooi, J. M. Guerrero, Designing high-order power-source synchronous current converters for islanded and grid-connected microgrids, Applied Energy 219 (2018) 370 – 384.

[15] W. Shi, X. Xie, C.-C. Chu, R. Gadh, Distributed optimal energy management in microgrids, IEEE Trans. Smart Grid 6 (3) (2015) 1137–1146.

[16] X. Lu, K. Sun, J. M. Guerrero, J. C. Vasquez, L. Huang, State-of-charge balance using adaptive droop control for distributed energy storage systems in DC microgrid applications, IEEE Trans. Ind. Electron. 61 (6) (2014) 2804–2815.

[17] T. Dragičević, J. M. Guerrero, J. C. Vasquez, D. Škrlec, Supervisory control of an adaptive-droop regulated DC microgrid with battery management capability, IEEE Trans. Power Electron. 29 (2) (2014) 695–706.

[18] S. Adhikari, F. Li, Coordinated Vf and PQ control of solar photovoltaic generators with MPPT and battery storage in microgrids, IEEE Trans. Smart Grid 5 (3) (2014) 1270–1281.

[19] N. L. Díaz, A. C. Luna, J. C. Vasquez, J. M. Guerrero, Centralized control architecture for coordination of distributed renewable generation and energy storage in islanded AC microgrids, IEEE Trans. Power Electron. 32 (7) (2017) 5202–5213.

[20] A. Mortezaei, M. Simoes, M. Savaghebi, J. Guerrero, A. Al-Durra, Cooperative control of multi-master-slave islanded microgrid with power quality enhancement based on conservative power theory, IEEE Trans. Smart Grid 9 (4) (2018) 2964–2975. doi:10.1109/TSG.2016.2623673.

[21] Q. Sun, J. Zhou, J. M. Guerrero, H. Zhang, Hybrid three-phase/single-phase microgrid architecture with power management capabilities, IEEE Trans. Power Electron. 30 (10) (2015) 5964–5977.

[22] D. Arcos-Aviles, J. Pascual, F. Guinjoan, L. Marroyo, P. Sanchis, M. P. Marietta, Low complexity energy management strategy for grid profile smoothing of a residential grid-connected microgrid using generation and demand forecasting, Applied energy 205 (2017) 69–84.

[23] M. A. Zehir, A. Batman, M. A. Sonmez, A. Font, D. Tsiamitros, D. Stimoniaris, T. Kollatou, M. Bagriyanik, A. Ozdemir, E. Dialynas, Impacts of microgrids with renewables on secondary distribution networks, Applied energy 201 (2017) 308–319.

[24] J. Li, R. Xiong, Q. Yang, F. Liang, M. Zhang, W. Yuan, Design/test of a hybrid energy storage system for primary frequency control using a dynamic droop method in an isolated microgrid power system, Applied Energy 201 (2017) 257–269.

[25] Y. Karimi, H. Oraee, M. S. Golsorkhi, J. M. Guerrero, Decentralized method for load sharing and power management in a PV/battery hybrid source islanded microgrid, IEEE Trans. Power Electron. 32 (5) (2017) 3525–3535.

[26] M. Kosari, S. H. Hosseinian, Decentralized reactive power sharing and frequency restoration in islanded microgrid, IEEE Trans. Power Syst. 32 (4) (2017) 2901–2912.

[27] D. Wu, F. Tang, T. Dragicevic, J. C. Vasquez, J. M. Guerrero, Autonomous active power control for islanded AC microgrids with photovoltaic generation and energy storage system, IEEE Trans. Energy Convers. 29 (4) (2014) 882–892.

[28] H. Mahmood, D. Michaelson, J. Jiang, Strategies for independent deployment and autonomous control of PV and battery units in islanded microgrids, IEEE J. Emerging Sel. Topics in Power Electron. 3 (3) (2015) 742–755.

[29] D. Wu, F. Tang, T. Dragicevic, J. C. Vasquez, J. M. Guerrero, A control architecture to coordinate renewable energy sources and energy storage systems in islanded microgrids, IEEE Trans. Smart Grid 6 (3) (2015) 1156–1166.

[30] Y.-S. Kim, E.-S. Kim, S.-I. Moon, Distributed generation control method for active power sharing and self-frequency recovery in an islanded microgrid, IEEE Trans. Power Syst. 32 (1) (2017) 544–551.

[31] Y. Xu, H. Sun, Distributed finite-time convergence control of an islanded low-voltage AC microgrid, IEEE Trans. Power Syst. 33 (3) (2018) 2339–2348. `doi:` `10.1109/TPWRS.2017.2743011`.

[32] A. Bidram, A. Davoudi, F. L. Lewis, J. M. Guerrero, Distributed cooperative secondary control of microgrids using feedback linearization, IEEE Trans. Power Syst. 28 (3) (2013) 3462–3470.

[33] J. W. Simpson-Porco, Q. Shafiee, F. Dörfler, J. C. Vasquez, J. M. Guerrero, F. Bullo, Secondary frequency and voltage control of islanded microgrids via distributed averaging, IEEE Trans. Ind. Electron. 62 (11) (2015) 7025–7038.

[34] L. Meng et al., Distributed voltage unbalance compensation in islanded microgrids by using a dynamic consensus algorithm, IEEE Trans. Power Electron. 31 (1) (2016) 827–838.

[35] V. Nasirian, Q. Shafiee, J. M. Guerrero, F. L. Lewis, A. Davoudi, Droop-free distributed control for AC microgrids, IEEE Trans. Power Electron. 31 (2) (2016) 1600–1617.

[36] P. Kofinas, A. Dounis, G. Vouros, Fuzzy Q-Learning for multi-agent decentralized energy management in microgrids, Applied Energy 219 (2018) 53 – 67.

[37] R. Han et al., Containment and consensus-based distributed coordination control to achieve bounded voltage and precise reactive power sharing in islanded AC microgrids, IEEE Trans. Ind. Appl. 53 (6) (2017) 5187–5199.

[38] R. Teodorescu, F. Blaabjerg, M. Liserre, P. C. Loh, Proportional-resonant controllers and filters for grid-connected voltage-source converters, IEE Proc. Elect. Power Appl. 153 (5) (2006) 750–762.

[39] Y. Gui, M. Li, J. Lu, S. Golestan, J. M. Guerrero, J. C. Vasquez, A voltage modulated DPC approach for three-phase PWM rectifier, IEEE Trans. Ind. Electron. 65 (10) (2018) 7612–7619. `doi:10.1109/TIE.2018.2801841`.

[40] H. Khalil, Nonlinear Systems, 3rd Edition, Prentice Hall, 2002.

[41] Y. Gu, W. Li, X. He, Passivity-based control of DC microgrid for self-disciplined stabilization, IEEE Trans. Power Syst. 30 (5) (2015) 2623–2632.

[42] Y. Gui, C. Kim, C. C. Chung, Improved low-voltage ride through capability for PMSG wind turbine based on port-controlled Hamiltonian system, Int. J. Control Autom. Syst. 14 (5) (2016) 1195–1204.

[43] F. Z. Peng, J.-S. Lai, Generalized instantaneous reactive power theory for three-phase power systems, IEEE Trans. Instrum. Meas. 45 (1) (1996) 293–297.

[44] Y. Gui, C. Kim, C. C. Chung, J. M. Guerrero, Y. Guan, J. C. Vasquez, Improved direct power control for grid-connected voltage source converters, IEEE Trans. Ind. Electron. 65 (10) (2018) 8041–8051. `doi:10.1109/TIE.2018.2801835.`

[45] Y. Gui, C. Kim, C. C. Chung, Grid voltage modulated direct power control for grid connected voltage source inverters, in: Amer. Control Conf., IEEE, 2017, pp. 2078–2084.

[46] J. M. Guerrero, M. Chandorkar, T.-L. Lee, P. C. Loh, Advanced control architectures for intelligent microgrids—Part I: Decentralized and hierarchical control, IEEE Trans. Ind. Electron. 60 (4) (2013) 1254–1262.

[47] X. Tang, W. Deng, Z. Qi, Investigation of the dynamic stability of microgrid, IEEE Trans. Power Syst. 29 (2) (2014) 698–706.

[48] R. Ortega, A. van der Schaft, B. Maschke, G. Escobar, Interconnection and damping assignment passivity-based control of port-controlled Hamiltonian systems, Automatica 38 (4) (2002) 585–596.

[49] H. Sira-Ramirez, Silva-Ortigoza, Control design techniques in power electronics devices, Springer-Verlag London Limited, 2006.

[50] Y. Gui, W. Kim, C. C. Chung, Passivity-based control with nonlinear damping for type 2 STATCOM systems, IEEE Trans. Power Syst. 31 (4) (2016) 2824–2833.

[51] L. Harnefors, A. G. Yepes, A. Vidal, J. Doval-Gandoy, Passivity-based controller design of grid-connected VSCs for prevention of electrical resonance instability, IEEE Trans. Ind. Electron. 62 (2) (2015) 702–710.

[52] A. C. Luna, N. L. Diaz, M. Graells, J. C. Vasquez, J. M. Guerrero, Mixed-integer-linear-programming-based energy management system for hybrid PV-wind-battery microgrids: Modeling, design, and experimental verification, IEEE Trans. Power Electron. 32 (4) (2017) 2769–2783.

[53] Microgrid technology research and demonstration, Aalborg University.
URL `http://www.meter.et.aau.dk`

[54] B. Wen, D. Boroyevich, R. Burgos, P. Mattavelli, Z. Shen, Analysis of DQ small-signal impedance of grid-tied inverters, IEEE Trans. Power Electron. 31 (1) (2016) 675–687.

[55] IEEE recommended practice and requirements for harmonic control in electric power systems, IEEE Std 519-2014 (Revision of IEEE Std 519-1992) (2014) 1–29`doi:10.1109/IEEESTD.2014.6826459`.